Songklanakarin J. Sci. Technol.
41 (4), 951-958, Jul. – Aug. 2019

http://www.sjst.psu.ac.th

*Original Article*

# Investigation of concrete material models for analysis of seismic behavior of reinforced concrete under reversed cyclic load

Rajendra Prasad Bohara[1], Ganchai Tanapornraweekit[2*], and Somnuk Tangtermsirikul[1]

[1] *School of Civil Engineering and Technology, Sirindhorn International Institute of Technology, Thammasat University, Khlong Luang, Pathum Thani, 12120 Thailand*

[2] *Construction and Maintenance Technology Research Center, School of Civil Engineering and Technology, Sirindhorn International Institute of Technology, Thammasat University, Khlong Luang, Pathum Thani, 12120 Thailand*

Received: 2 March 2018; Revised: 8 May 2018; Accepted: 17 May 2018

## Abstract

Several concrete material models with unique theoretical backgrounds are available in different finite element analysis (FEA) software packages such as ABAQUAS, ATENA, DIANA, and LS-DYNA. In the simulation of structural responses of concrete using FEA software, various parameters such as strength, stiffness, softening, strain rate, and dilation are required to be provided. Though depending on each concrete material model, all of these parameters do not hold equal importance during a single type of loading. This paper presents the relevance of using the three most widely used concrete material models available in LS-DYNA: Karagozian & Case Concrete (KCC) model, Winfrith Concrete Model, and Continuous Surface Cap Model (CSCM) for simulation of concrete structures under reversed cyclic loading when only limited material properties are available. In this paper, a series of nonlinear 3D-finite element analyses of non-ductile reinforced concrete (RC) column subjected to lateral cyclic loading were carried out with these three concrete models. The results from each model were compared with documented experimental results. The capacity of each material model to capture the cyclic load reversal behavior, softening due to cyclic compression and tension, and damages are the major foci of this paper. Based on a series of numerical analyses of an RC column under cyclic loading, review of a single element analysis, and a theoretical overview of each model, recommendations for the selection of an appropriate concrete material model under cyclic loading were made.

**Keywords:** CSCM model, FEA, KCC model, seismic loading, Winfrith Concrete

## 1. Introduction

Concrete is the most widely used material for structures all over the globe. Concrete structures are required to resist various types of loads such as gravity, earthquake, wind and sometimes blast, and impact loadings. In order to ensure the safety and reliability of the structures against these actions, various laboratory experiments have been carried out. However, most of structural load tests, especially for full scale structures, require extensive resources, i.e. lab facilities as well as budget and time (Sharath, Arumugam, Dhana sekaran, & Subash, 2017; Wu, Crawford, Magallanes, & Way, 2012). These reasons require simulation of structural responses using a finite element analysis (FEA) software package which is a better alternative to obtain quick and reliable results. However, it is worth pointing out that improper use of a FEA leads to inaccurate prediction of structural performance which results from various reasons, e.g., inappropriate selection of material models and their parameters, as well as boundary conditions. Therefore, this paper emphasizes the behavior of concrete material models subjected to seismic loading so that appropriate selection of a concrete material model for seismic loading can be suggested.

Earthquake, which causes the dynamic actions on structures, is a displacement-type loading (Murthy, Rupen,

*Corresponding author
Email address: ganchai@siit.tu.ac.th

Vijayanarayanan, & Mehta, 2012). Most of the seismic loading problems are simulated using displacement controlled lateral cyclic loading so that nonlinear behavior is able to be captured. A comprehensive material model to take into account the cyclic behavior and the softening plays a vital role for the simulation of structures subjected to lateral cyclic loading.

LS-DYNA, a high fidelity FE code, has been used to analyze large deformation response of structures under both static and dynamic loadings (Hallquist, 2006). The current version of LS-DYNA is rich in material models. It contains more than 270 material models and approximately 100 of them are constitutive models governed by ten equations-of-state to cover a broad spectrum of materials (Hallquist, 2006; Livemore Technology Software Corporation [LSTC], 2016). Furthermore, among the constitutive models, several constitutive concrete material models are available with some pros and cons in each.

In LS-DYNA, much research has been carried out to validate various material models for different loads such as quasi static, blast, and impact (Coleman, 2016). However, the number of research studies is limited on the simulation of structures under earthquake load using LS-DYNA. Coleman (2016) evaluated the cyclic performance of four commonly used LS-DYNA concrete materials, i.e. KCC, Winfrith Concrete, CSCM, and RTH, in single-element and multi-element analysis with respect to element size, strain application, hourglass, and element formulation in explicit solver. This was the only document found which focused completely on seismic behavior of different concrete material models.

This present paper focuses on the behavior of the three most widely used concrete material models, i.e. KCC model, Winfrith Concrete Model, and the CSCM, under lateral cyclic loading. In this paper, a series of nonlinear finite element analyses of a non-ductile reinforced concrete (RC) column under lateral cyclic loading were carried out with three different material models using implicit solver to investigate the cyclic and softening behavior due to cyclic compression and tension. The results from each material model were compared with previously reported laboratory results. A recommendation on the selection of an appropriate material model is made based on three platforms: numerical analysis, review of single element analysis, and theoretical background.

## 2. Experimental Program

A non-ductile RC column of cross section 350×250 mm and shear span of 2050 mm, previously tested by Rosdin, Warnitchai, and Awan (2010) and numerically analyzed by Saleem, Pimanmas, and Mehmood (2015) using VecTor2 software (a non-linear FE program developed at the University of Toronto), was selected as a case for verification of concrete material models. This type of column is commonly found in low-rise buildings in Thailand. The column consisted of 12-DB16 as longitudinal reinforcement and two closed loops of RB6@200 mm as stirrups. The column cross section and reinforcement details are shown in Figure 1.

30 MPa compressive strength concrete was used for the column. The mechanical properties of the reinforcement are summarized in Table 1. The column was constructed on a base RC block, which was designed to remain elastic throughout the experiment and was firmly fixed with a rigid floor. A constant vertical load of 400 kN was applied on the top of the column until the end of the experiment. Incremental drift ratios (±0.25%, ±0.50%, ±0.75%, ±1.0%, ±1.5%, ±2.0%, ±2.5%, and ±3.0%) with two cycles of each drift ratio were applied using a hydraulic actuator.

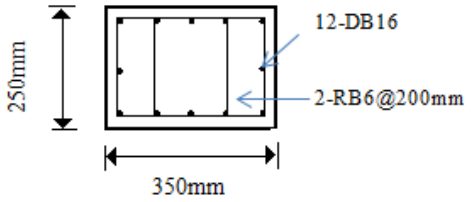


Figure 1. Cross section of column (Rosdin *et al.*, 2010).

Table 1. Mechanical properties of rebars (Rodsin *et al.*, 2010).

| Bar size | Modulus of elasticity (GPa) | Yield strength (MPa) |
|---|---|---|
| DB12 | 204 | 547 |
| RB9 | 204 | 396 |

## 3. FEA Methodology

Both the column and base block were modeled with solid brick elements (eight node hexahedron). Rebars were modeled as beam elements, which were constrained in the concrete so that a perfect bonding between reinforcement and concrete was obtained. Based on the mesh convergence study, a uniform mesh size of 50 mm was adopted for both solid and beam elements. In order to simulate cast-in-situ behavior, the nodes of base block and column were merged together on the common overlapping surface. The bottom nodes of the base block were assigned to be hinge support and implicit solver was utilized to obtain a quasi-static solution. The analyzed FE model is presented in Figure 2.

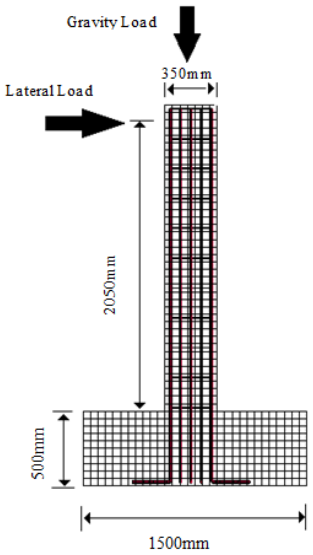


Figure 2. Finite element meshes of the analyzed specimen.

The gravity load was applied on top of the column, which was distributed uniformly to the column cross section. This gravity load was ramped for 3 seconds until it attained its peak value of 400 kN and then held constant until the termination time. The ramping of load was used in order to prevent a probable divergence in implicit solver. The lateral displacement cycle began only after 3 seconds following the same incremental drifts as employed in the experimental study.

## 4. Material Input Parameters

Depending on the material models, each model had different minimum input parameters, which is explained in sections 4.1 to 4.3. As only the compressive strength of the concrete (30 MPa) was known, the general values of the other concrete properties were adopted as follows: mass density (2400 kg/m$^3$), Poisson's ratio (0.19), and aggregate size (19 mm). It was noted that for each material model only the minimum required inputs were provided for each analysis since this study investigated the performance of each concrete model when only limited material properties are known.

Steel reinforcement in the column was defined according to the Plastic Kinematic Model (MAT_003), which is suitable for the simulation of both isotropic and kinematic hardening plasticity (LSTC, 2016). As recommended by Hallquist (2009) for cyclic loading, the mixed hardening approach with a hardening parameter of 0.3 was used.

### 4.1 KCC model: MAT_72R3

Although this material model has 49 input parameters provided in eight keyword cards, it was not necessary to input all of them by the user for general purposes. This model can auto-generate all of the parameters based on the provided density and compressive strength of concrete. Therefore, only the compressive strength and density of concrete along with unit conversion parameters were input into the model and other parameters were set to default values. Details on the simplified input for the KCC model can be found in Schwer and Malvar (2005).

### 4.2 Winfrith concrete model: MAT_84

Compared to the KCC model, more parameters need to be defined for the Winfrith Concrete Model. However, these parameters can be obtained through tests or calculation based on various design codes. This paper adopted the ACI 318-08 (ACI Committee 318 2008) for such calculations.

The crack generation up to three orthogonal planes in a single element is one of the appealing features of this model, which is utilized in strain softening during tension. However, as reported by Schwer (2011), in cyclic tension and compression, the tensile cracks opened during tension were found to be healed during subsequent compression and no softening was observed after compression failure. In addition, according to Wu *et al.* (2012) Winfrith Concrete is able to capture the post-peak softening in tension but not in compression.

The input parameters for this concrete model were mass density, initial tangent modulus, Poisson's ratio, uniaxial compressive strength, uniaxial tensile strength, and fracture energy.

### 4.3 CSCM: MAT_159

Similar to the KCC model, this model also has features to generate the required parameters based on unconfined compressive strength (LSTC, 2016). According to Jiang and Zhao (2014), the CSCM (MAT_159) is applicable only for concrete with a compressive strength in the range of 20 MPa to 48 MPa. For concrete with a compressive strength out of this range, the MAT_SCHWER_MURRAY_CAP_MODEL (MAT_145) can be used. However, MAT_145 has no inbuilt parameter generation feature.

Similar to other material models, the compressive strength of concrete was defined to be 30 MPa, which is also the default value in this model. Further, the cap retraction was turned on and modulus recovery option was turned off in the analysis performed in this study.

## *5.* Results and Discussion

In order to investigate the cyclic load reversal and softening behavior of different material models, the force-drift (backbone) curves obtained from all simulations were compared (Figure 3). Although the force was expected to drop after reaching the maximum value, it continued to increase for the Winfrith and KCC models even after exceeding the peak force that resulted from the experiment. However, the force was relatively smaller in the KCC model compared to the Winfrith Concrete Model and a gradual drop in the force was observed in the KCC model at very high drift (Figure 3). Among these materials, the CSCM was the only material to show a drop in force at the expected drift level, which was similar to the experimental results. During the early cycles (the elastic range), all of the models showed approximately an equal force output (Figure 3). Then, a clear gap between the peak force values, with increased drift, from different material models could be observed from the analysis results. Further, the KCC model and CSCM showed approximately the same force output up to the maximum force level. It was noted that all models are able to capture the cyclic reversal loading.

Although no gradual drop in the force was observed in the Winfrith Concrete Model, the rate of force rising was not the same. It gradually decreased with increasing drift. This behavior was expected due to crack formation in tension and then, healing in compression during cyclic loading as explained by Schwer (2011).

The Winfrith Concrete Model is based on the Ottosen Plasticity Model (Ottosen, 1977), which expresses the shear failure surface as:

$$f(I_1, J_2, \cos 3\theta) = A\frac{J_2}{f'^2_c} + \lambda\frac{\sqrt{J_2}}{f'_c} + B\frac{I_1}{f'_c} - 1 \quad (1)$$

where, $I_1$, $J_2$, $\theta$, and $f'_c$ represent first invariant stress tensor, second deviatoric stress tensor, lode angle, and unconfined compressive strength of concrete, respectively.

This expression is also known as the four-parameter model. Parameters A and B account for meridional shape of

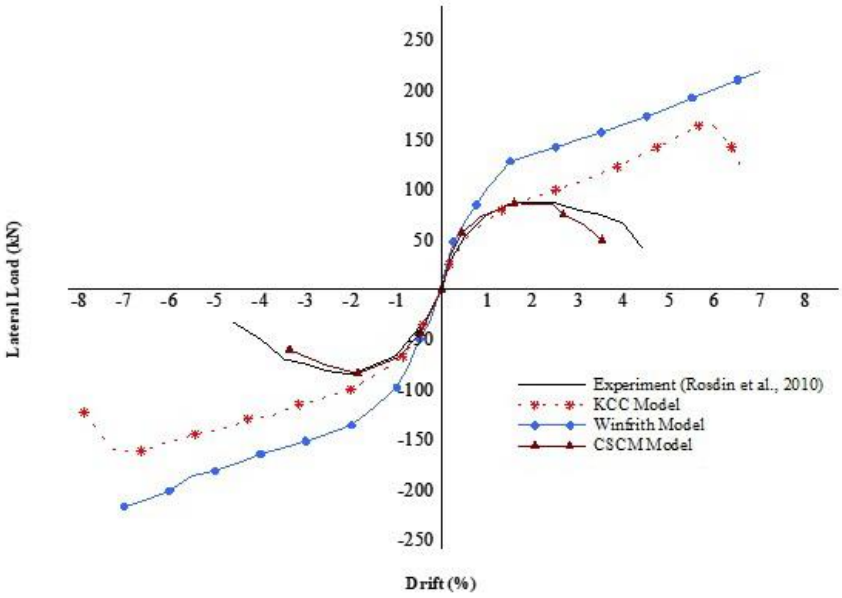


Figure 3. Comparison of force-drift (backbone curves) from experiment and analyses using different concrete material models.

shear failure surface and λ controls the shape of the shear failure surface on the π-plane (Schwer, 2011). Further, λ is a function of cos3θ which is expressed as:

$$\lambda = \begin{cases} K_1 \cos\left[\frac{1}{3}\cos^{-1}(K_2 \cos 3\theta)\right] & \text{for } \cos 3\theta \geq 0 \\ K_1 \cos\left[\frac{\pi}{3} - \frac{1}{3}\cos^{-1}(-K_2 \cos 3\theta)\right] & \text{for } \cos 3\theta \geq 0 \end{cases} \quad (2)$$

The parameters $K_1$ and $K_2$ are known as size and shape factors, respectively. The values of failure criteria parameters A, B, $K_1$, and $K_2$ are functions of the ratio of tensile strength to compressive strength of concrete. In the Winfrith Concrete Model, strain softening in tension is carried out by regularization of crack widths or fracture energy. However, its crack healing behavior in cyclic loading (Schwer, 2011) prevents the actual rate of softening in this type of loading. Further, it should be noted that the concrete failure criteria in the Ottosen plasticity model (Ottosen, 1977) was originally validated for short-term monotonic loading.

Behavior of the KCC model and CSCM are more or less similar, though the KCC model over predicted the resistant force. In generalized form, both the KCC model and CSCM are expressed in three shear strength surfaces: yield surface, limit surface, and residual surface (Brannon & Leelavanichkul 2009) (Figure 4).

With respect to Figure 4, the softening is defined as the gradual shifting of limit surface to the residual surface. In other words, some stress attained once can never be reached again due to softening.

The three surfaces of the KCC model are defined as:

Initial Yield Surface, $$Yy = a_{0y} + \frac{p}{a_{1y} + a_{2y} p} \quad (3)$$

Limit Surface, $$Ym = a_{0m} + \frac{p}{a_{1m} + a_{2m} p} \quad (4)$$

Residual Surface, $$Yr = a_{0f} + \frac{p}{a_{1f} + a_{2f} p} \quad (5)$$

The a-parameters ($a_{0y}$, $a_{1y}$, $a_{1y}$, $a_{0m}$, $a_{1m}$, $a_{2m}$, $a_{0f}$, $a_{1f}$ and $a_{2f}$) are the user input values for initial yield, limit and residual surfaces, and p is the pressure, which can be expressed as $-I_1/3$.

The failure surface is interpolated between $Y_m$ or $Y_r$ depending on the following conditions:

$$f(I_1, J_2, J_3) = \begin{cases} r(J_3)\left[\eta(\lambda)\left(Y_m(p) - Y_y(p)\right) + Y_y(p)\right] & for\ \lambda \leq \lambda_m \\ r(J_3)\left[\eta(\lambda)\left(Y_m(p) - Y_r(p)\right) + Y_r(p)\right] & for\ \lambda > \lambda_m \end{cases} \quad (6)$$

where $\lambda$ is the modified effective plastic strain which accounts for internal damage and is defined in Equation 7. $r(J_3)$ is a function of the third devioteric stress serving as a scale factor in the form of the William-Warnke Equation (William & Warnke, 1975). In the KCC model, rate effects are used to take into account shear damage accumulation. A factor $r_f$, (strain rate enhancement factor), termed as the dynamic increasing factor (DIF) in CEB-FIB Model Code 90, is implemented to account for high loading rates.

$$\lambda = h \sqrt{\frac{2}{3} \varepsilon_{ij}^{\ p} \varepsilon_{ij}^{\ p}} \quad (7)$$

where $\varepsilon_{ij}^{\ p}$ is the strain tensor. The parameter h, which is the function of softening parameters, tensile strength of concrete, pressure and DIF, is expressed as:

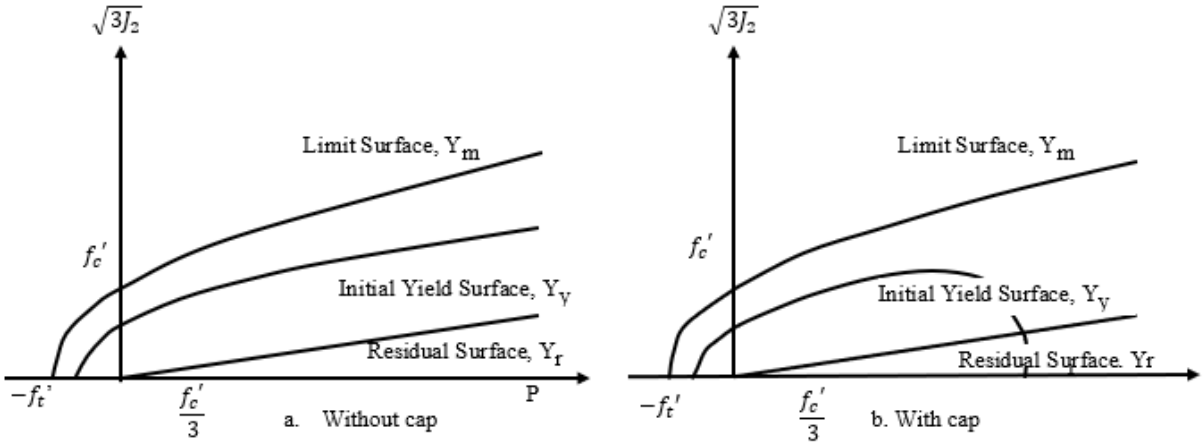


Figure 4. Strength surfaces (Brannon & Leelavanichkul, 2009).

$$h=\begin{cases}\dfrac{1}{r_f\left(1+\frac{p}{r_f f_t}\right)^{b_1}} & for\ compression\ (p \geq 0)\\ \dfrac{1}{r_f\left(1+\frac{p}{r_f f_t}\right)^{b_2}} & for\ tension\ (p<0)\end{cases} \quad (8)$$

The parameters $b_1$ and $b_2$ account for softening in compression and tension, respectively. Despite having the softening parameters in the KCC model, a significant difference in the resistant forces between experiment and simulation still existed. The main reason for this difference possibly resulted from an adoption of the auto parameter generation feature. When only the unconfined compressive strength and density of concrete are defined as inputs, the curve for strain rate effects (LCRATE in keyword Card 3) is not generated, which holds paramount importance in softening and damage accumulation. As a result, softening is not well simulated because the actual rate and higher force output are shown.

The CSCM, which is an elasto-plastic damage model, is based on formulations purposed by Schwer and Murray (1994) and Sandler, DiMaggio, and Baladi (1976). The yield function of this model can be expressed as three invariants as follows (LSTC, 2016):

$$Y(I_1, J_2, J_3) = J_2 - R(J_3)^2 f_f^2(I_1) f_c(I_1, k) \quad (9)$$

where $R(J_3)$ represents the Rubin three-invariant reduction factor, $f_f(I_1)$ is the shear failure surface, and $f_c(I_1, k)$ represents the hardening cap with $k$ as the cap hardening parameter, which are defined as follows:

Shear Failure Surface,

$$f_f(I_1) = \alpha - \lambda(\exp)^{-\beta I_1} - \theta I_1 \quad (10)$$

Cap Hardening Surface,

$$f_c(I_1, k) = 1 - \frac{(I_1 - L(k))^2}{(X(k) - L(k))^2} \quad for\ I_1 \geq L(k)$$
$$= 1 \quad otherwise \quad (11)$$

$$L(k) = \begin{cases} k & for\ k \geq k_0 \\ k_0 & otherwise \end{cases} \quad (12)$$

$$X(k) = L(k) + Rf_f(I_1) \quad (13)$$

where the material parameters α, β, θ, and λ are based on triaxial compression tests on plain concrete and then, the parameters are adjusted for compaction and damage (Murray, 2007). $f_f$ $(I_1)$, and $f_c$ $(I_1, k)$ intersect at $I_1 = L(k)$. Further, Equation 11 depicts an ellipse when $I_1 \geq L(k)$ and R is the cap ellipticity. Equation 13 governs the location of cap. Moreover, increased values of $X(k)$ and $k$ indicate expansion of the cap and vice-versa. Also, the following hardening rule is implemented to control the motion of the cap:

Plastic volumetric strain,

$$\varepsilon_v^p = W\left[1 - \exp^{(-D_1(X-X_0) - D_2(X-X_0)^2}\right] \quad (14)$$

where W is the maximum value of volumetric strain and $X_0$ represents the initial location of the cap (when $k = k_0$). $D_1$ and $D_2$ are the model input parameters.

Unlike the KCC model, the CSCM has inbuilt functions that take into account the DIF during both tension and compression. Two separate equations (Equation 15 and Equation 16) are implemented to capture the softening during brittle and ductile damage with softening parameters A, B, C, and D (LSTC, 2016).

Brittle damage,

$$d(\tau_b) = \frac{0.999}{D}\left[\frac{1+D}{1+D\exp^{-C(\tau_b - r_0 b)}} - 1\right] \quad (15)$$

Ductile damage,

$$d(\tau_d) = \frac{dmax}{B}\left[\frac{1+B}{1+B\exp^{-A(\tau_b - r_0 d)}} - 1\right] \quad (16)$$

where,

Brittle damage accumulation, $\tau_b = \sqrt{E\,\varepsilon^2{}_{max}}$ (17)

Ductile damage accumulation, $\tau_d = \sqrt{\frac{1}{2}\sigma_{ij}\varepsilon_{ij}}$ (18)

where $\sigma_{ij}$ and $\varepsilon_{ij}$ are the stress and strain components, respectively.

Viscoplastic damage threshold,

$$r_0 = \left(1 + \frac{E\dot{\varepsilon}\eta}{r^s\sqrt{E}}\right) r^s \quad (19)$$

where $r_0 b$ and $r_0 b$ in Equation 15 and Equation 16 are the threshold brittle and ductile damage parameters. The damage initiates only when $\tau_b$ and $\tau_d$ exceed respective thresholds. $r^s$ and $r_0$ represent damage threshold before and after application of viscoplasticity.

Using all the inbuilt parameters, the CSCM was able to capture softening behavior and predict peak load and respective drift of a non-ductile column with good accuracy. The hysteresis curve obtained from the CSCM compared to the experimental hysteresis curve is presented in Figure 5.

Peak load from the experiment was 86.83 kN at around 2% drift and the peak load predicted by FEA was 85.82 kN at the same level of drift. The numerical modeling in VecTor2 by Saleem *et al.* (2015) reported the maximum load to be 89.1 kN at around 2% drift.

Regarding the damage patterns that resulted from the analyzed models, the fringes of the maximum principal strains at 3% drift are presented in Figure 6. Based on maximum principal strain, the KCC model over predicted the damage and the Winfrith Concrete Model showed the least damage. Again, the CSCM captured damages with good accuracy compared to the test results.

On the basis of maximum plastic strain, the damage zone and damage propagation could be identified. However, it is rather unclear to specify which element failed first and gets damaged earlier. Therefore, the CSCM was run again with activation of its inbuilt erode option. Activation of this option eliminated the failed elements from the model (LSTC, 2016). Damage obtained from this model is presented in Figure 7 which shows good resemblance to the damage shown in the experiment (Rosdin *et al.*, 2010).

In order to evaluate the energy dissipated during reversed lateral cyclic loading, the areas enclosed within the hysteresis loops at various drift ratios were calculated. The comparison of energy dissipated during the cycles of different drifts as well as the cumulative energy dissipation from both experiments (Rosdin *et al.*, 2010) and the FEA are presented in Figure 8. During the early cycles, the FE model was able to capture the energy dissipation with good accuracy. However, a comparison of cumulative energy dissipation up to 3.5% drift showed that the FE model over predicted the energy by 10.48%.

In the experiment, longitudinal rebar buckling was observed at the lateral drift of 3% and the column ultimately collapsed by flexural mode of failure (Saleem *et al.*, 2015). Similar to the experiment, buckling in the longitudinal rebars was shown at 3% drift in numerical simulation as well. Figure 9 presents the development of axial stress in longitudinal rebars with respect to increased drift at the buckling location of the longitudinal rebars. The main longitudinal rebars at the corner along the loading direction started buckling at 3% drift. As the relationship of axial stress of both the rebars and drift ratio showed similar behavior, a single curve is presented in Figure 9. Buckling in the rebars can be identified with the rapid drop in axial compressive stress at 3% drift (Figure 9). Buckling of rebars and excessive damage in the concrete led the model to numerical instability and no convergence was obtained after 3.5% drift.

Among the simulated material models, the performance of the CSCM was excellent regarding prediction of peak load and corresponding drift level as well as damage

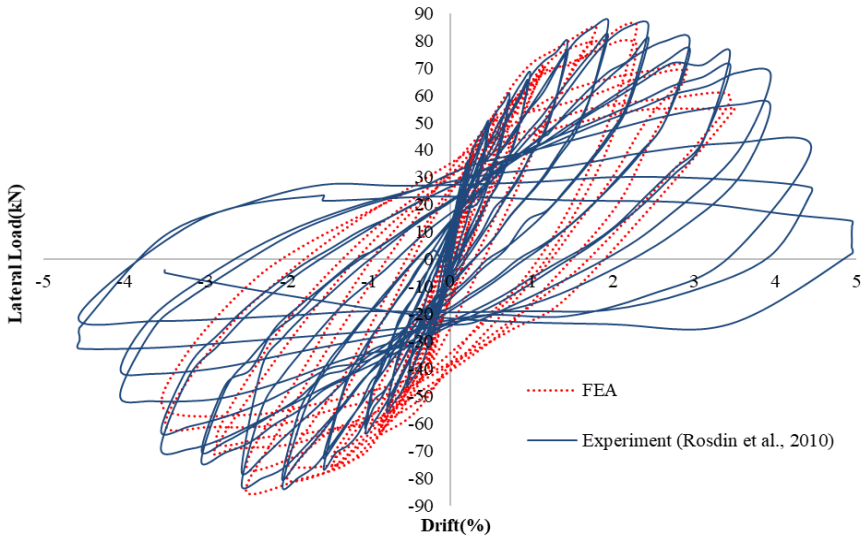


Figure 5. Comparison of force-drift (hysteresis curves) from experiment and analysis using CSCM concrete model.

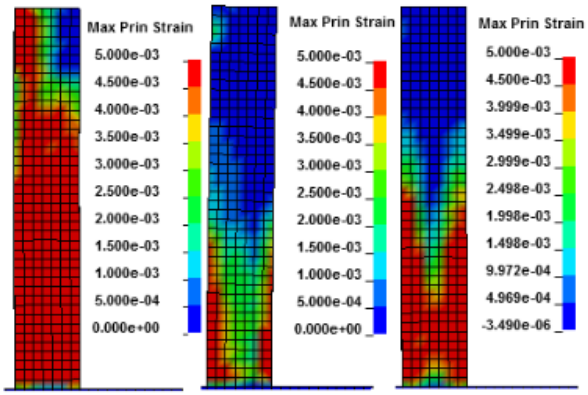


a. KCC model b. Winfrith model c. CSCM model

Figure 6. Fringes of maximum principal strain.

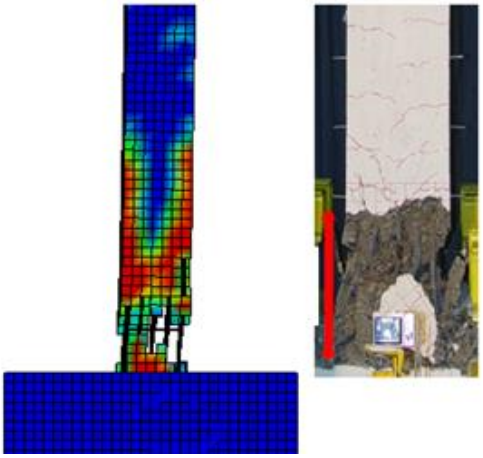

a. CSCM model with erode option b. Experiment (Rodsin *et al.*, 2010)

Figure 7. Comparison of damage patterns.

level when only the minimum required input parameters are defined. However, energy dissipitaion capacity predicted by the CSCM (with mimimum input parameters) differed from the experiment in the post-peak regime. The predicted energy dissipation capacity by FEA was good up to 1.5% drift. After 1.5% drift local yeilding occurred in both longitudinal and lateral ties at critical locations and significant flexural damage was observed in the column. With the increased level of damage, relatively larger deviataions in energy dissipated by the FEA and experiment were obseved.

## 6. Conclusions

This paper evaluates the seismic performance of three widely used concrete material models (KCC model, Winfrith Concrete Model, and the CSCM) with minimum input parameters using implicit solver provided by LS-DYNA FE code. The selected specimen used for comparison was a previously tested non-ductile RC column under lateral cyclic loading. The results from the simulation with three different material models were compared with the experimental results. Finally, the obtained results from each material model were investigated together with an overview of theoretical background and documented single element analysis. Based on this study, the following conclusions can be drawn.

All concrete material models used in this study were able to capture the cyclic load reversal behavior during application of cyclic displacements. However, only the CSCM showed the softening with good accuracy and consequently, predicted reliable force-displacement behavior and damage pattern. Therefore, on the basis of theoretical background, and comparison of experimental and simulation results, this paper recommends the CSCM (MAT_159) for lateral cyclic loading simulation when only the compressive strength of the concrete is known.

An overview of the theory of the KCC model shows its potential for a simulation of softening in concrete. However, due to the lack of automatically generated DIF input, the softening behavior, which is a function of strain rate, could not be simulated well and no reliable force-displacement output could be obtained when only the density and compressive strength of the concrete were input in the material keyword cards. Also, the cyclic behavior of this material model is not as good as those of others and excessive maximum principal strain (damage) formation is another disadvantage of this model. However, it should be noted here again that this investigation is based on the minimum input with auto-generation parameters. The inputs were only density and compressive strength of concrete for the KCC model.

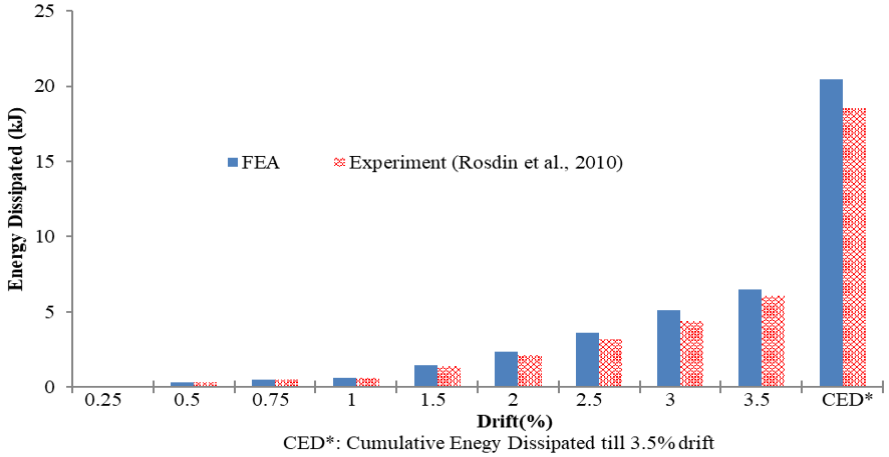


CED*: Cumulative Enegy Dissipated till 3.5% drift

Figure 8. Comparison of energy dissipated.

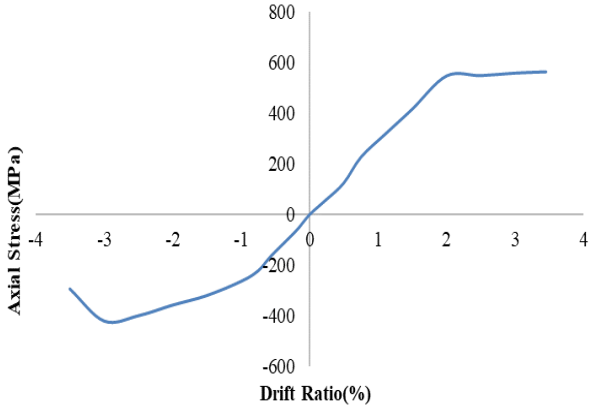


Figure 9. Axial stress in longitudinal rebars vs. drift ratio.

In the Winfrith Concrete Model, no softening in compression was observed during cyclic loading. As a result, among the three evaluated material models, this model showed the maximum force output and least maximum principal strain (damage). Therefore, this material model is not recommended for simulation of concrete under cyclic loading when significant damage is expected.

## Acknowledgements

The first author would like to express his appreciation to the Excellent Foreign Student (EFS) Scholarship and the TU Scholarship for Foreign Students for the opportunity to pursue my MS degree at Sirindhorn International Institute of Technology (SIIT), Thammasat University.

## References

American Concrete Institute, and International Organization for Standardization. (2008). *Building code requirements for structural concrete (ACI 318-08) and commentary*. Oakland, MI: American Concrete Institute.

Brannon, R. M., & Leelavanichkul, S. (2009). Survey of four damage models for concrete. *Sandia National Laboratories*, *32*(1), 1-80. Retrieved from http://prod.sandia.gov/techlib/access-control.cgi/2009/095544.pdf

Coleman, D. K. (2016). *Evaluation of concrete modeling in LS-DYNA for seismic application* (Master's thesis, The University of Texas at Austin, Austin, TX). Retrieved from https://repositories.lib.utexas.edu/handle/2152/47239

Hallquist, J. O. (2006). *LS-DYNA theory manual.* Livemore, CA: Livemore Technology Software Corporation.

Hallquist, J. (2009). *Recent developments in LS-DYN A.* Livemore, CA: Livemore Technology Software Corporation.

Jiang, H., & Zhao, J. (2015). Calibration of the continuous surface cap model for concrete. *Finite Elements in Analysis and Design*, *97*, 1-19.

Livemore Technology Software Corporation. (2016). *LS-DYNA keyword mannual, Vol. II*. Livemore, CA: Author.

Murray, Y. D. (2007). *Users manual for LS-DYNA concrete material model 159* (No. FHWA-HRT-05-062). Retrieved from https://www.fhwa.dot.gov/publications/research/infrastructure/pavements/05062/05062.pdf

Murty, C. V. R., Goswami, R., Vijayanarayanan, A. R., & Mehta, V. V. (2012). *Some concepts in earthquake behavior of buildings*. Gujarat, India: Gujarat State Disaster Management Authority, Government of Gujarat. Retrieved from http://www.iitk.ac.in/nicee/IITK-GSDMA/EBB_001_30May2013.pdf.

Ottosen, N. S. (1977). A failure criterion for concrete. *American Society of Civil Engineers. Engineering Mechanics Division. Journal*, *103*(4), 527-535.

Rodsin, K., Warnitchai, P., & Awan, T. (2010). Ultimate drift at gravity load collapse of non-ductile RC columns. *5th Civil Engineering Conference in the Asian Region and Australasian Structural Engineering Conference*, Sydney Australia (p. 441).

Saleem, S., Pimanmas, A., & Mehmood, T. (2015). Finite element modeling of non-ductile reinforced concrete columns. *Engineering Journal of Research and Development*, *26*(1), 23-34.

Sandler, I. S., Dimaggio, F. L., & Baladi, G. Y. (1976). Generalized cap model for geological materials. *Journal of Geotechnical and Geoenvironmental Engineering*, *102*.

Schwer, L. (2011). The Winfrith concrete model: Beauty or beast? Insights into the Winfrith concrete model. *Proceeding of the 8th European LS-DYNA Users Conference* (pp. 23-24). Strasbourg, France.

Schwer, L. E., & Malvar, L. J. (2005). Simplified concrete modeling with* MAT_CONCRETE_DAMAGE_REL3. *JRI LS-Dyna User Week*, 49-60.

Schwer, L. E., & Murray, Y. D. (1994). A three-invariant smooth cap model with mixed hardening. *International Journal for Numerical and Analytical Methods in Geomechanics*, *18*(10), 657-688.

Sharath, R., Arumugam, D., Dhanasekaran, B., & Subash, T. R. (2017). Numerical modeling of 'concrete response' to high strain rate loadings. *Proceeding of the 11th European LS-DYNA User Conferene*. Salzburg, Austria.

Telford, T. (1990). *CEB-FIB model code. Design code edition*, Lausanne, Switzerland: The International Federation for Structural Concrete.

William, K. J., & Warnke, E. P. (1975). Constitutive model for the triaxial behavior of concrete. *Proceeding of ISMES Seminar on Concrete Structures Subjected to Triaxial Stresses.* Bergamo, Italy.

Wu, Y., Crawford, J. E., & Magallanes, J. M. (2012). Performance of LS-DYNA concrete constitutive models. *Proceeding of the 12th International LS-DYNA Users Conference* (pp. 3-5). Detroit, MI.